

Deep source separation of overlapping gravitational-wave signals and non-stationary noise artifacts

Niklas Houba

*ETH Zurich, Department of Physics, Institute for Particle and Astrophysics,
Wolfgang-Pauli-Str. 27, 8093 Zurich, Switzerland*

The Laser Interferometer Space Antenna (LISA) will observe gravitational waves in the millihertz frequency band, detecting signals from a vast number of astrophysical sources embedded in instrumental noise. Extracting individual signals from these overlapping contributions is a fundamental challenge in LISA data analysis and is traditionally addressed using computationally expensive stochastic Bayesian techniques. In this work, we present a deep learning-based framework for blind source separation in LISA data, employing an encoder-decoder architecture commonly used in digital audio processing to isolate individual signals within complex mixtures. Our approach enables signals from massive black-hole binaries, Galactic binaries, and instrumental glitches to be disentangled directly in a single step, circumventing the need for sequential source identification and subtraction. By learning clustered latent space representations, the framework provides a scalable alternative to conventional methods, with applications in both low-latency event detection and full-scale global-fit analyses. As a proof of concept, we assess the model’s performance using simulated LISA data in a controlled setting with a limited number of overlapping sources. The results highlight deep source separation as a promising tool for LISA, paving the way for future extensions to more complex datasets.

I. INTRODUCTION

The Laser Interferometer Space Antenna (LISA) is a space-borne gravitational-wave observatory developed by the European Space Agency (ESA) in collaboration with NASA, scheduled for launch in the mid-2030s [1]. The detector consists of three spacecraft nominally arranged in an equilateral triangle, with each pair separated by 2.5 million kilometers [2]. Using laser interferometry, LISA will measure fluctuations in spacetime caused by passing gravitational waves, extending the pioneering observations of ground-based detectors such as the Laser Interferometer Gravitational-Wave Observatory (LIGO) and Virgo [3–13].

Unlike terrestrial detectors, which are constrained by seismic noise at low frequencies, LISA’s space-borne configuration enables the detection of gravitational waves in the 0.1 mHz to 1 Hz frequency band, a region densely populated with gravitational-wave sources [14, 15].

A. Challenges in LISA data analysis

LISA’s sensitivity to millihertz sources will produce a data stream comprising a superposition of millions of overlapping gravitational-wave signals. Among these, Galactic binaries (GBs) – and particularly double white-dwarf systems – are expected to be so numerous that they will create an astrophysical noise floor, posing substantial challenges for scientific data analysis [16, 17]. While a subset of sources, numbering in the tens of thousands, will be individually resolvable, the majority will blend into a persistent foreground noise, complicating the detection and characterization of other signals, including transient events from merging massive black-hole binaries (MBHBs). Instrumental noise further exacerbates

the difficulty of disentangling individual sources [18–20]. Addressing this challenge, known as the global-fit problem, requires high-performance, scalable data analysis algorithms capable of efficiently identifying and characterizing LISA’s targets.

Solving the astrophysical global-fit problem requires methods that identify, model, and analyze gravitational-wave sources within a unified framework. Current approaches include Bayesian Markov Chain Monte Carlo (MCMC) and Maximum Likelihood Estimation (MLE) [21–23]. Both techniques have been successfully applied to simulated LISA datasets, each offering distinct trade-offs in computational cost, accuracy, and adaptability. MCMC-based global fits, such as Erebor or GLASS, leverage ensemble sampling and GPU or parallel-CPU acceleration for improved efficiency [21, 22]. These pipelines further rely on reversible-jump MCMC [24] to handle the uncertain number of sources in the data. To enhance computational efficiency, global-fit frameworks are structured to run large sampler modules covering a subset of sources in a blocked Gibbs fashion [25, 26]. The approach ensures a consistent treatment of overlapping sources, but remains computationally demanding, potentially limiting its near-real-time application.

In contrast, MLE-based methods adopt a step-wise signal extraction process, estimating and subtracting sources like MBHBs, before analyzing GBs [23, 27]. This approach enables dynamic updates as new data arrives. However, uncertainty estimates are obtained from the Fisher information matrix, and thus are limited by the implicit assumption of Gaussian distributions without source correlations, though MCMC refinements can improve accuracy.

Given these challenges, research into complementary approaches for source separation in LISA data remains an active and evolving field. Deep-learning methods for

data-driven feature extraction present a promising alternative by enabling direct source separation in a single step. These techniques offer advantages in computational efficiency, architectural flexibility, and scalability. The deep source separation approach holds potential for both low-latency applications and global-fit analyses.

B. Source separation in science and engineering

The task of untangling overlapping signals from a complex mixture remains both essential and challenging across various scientific and engineering disciplines [28–30]. Imagine walking through a bustling city street, where car horns, music from storefronts, and conversations blend into a chaotic soundscape. While the human brain can effortlessly isolate specific voices or familiar sounds, digital audio processing struggles to achieve similar performance.

Early approaches leveraged statistical techniques such as Independent Component Analysis (ICA) to separate mixed signals mathematically [31]. ICA operates under the assumption that the underlying sources are statistically independent, seeking a transformation that maximizes their separation. This is typically accomplished by expressing the observed mixed signals as a linear combination of unknown independent sources and estimating a separation matrix to recover the original signals without requiring prior knowledge of their specific characteristics. Beamforming methods, on the other hand, use microphone arrays to spatially isolate sound sources, similar to how directional microphones enhance a speaker’s voice in a noisy environment by focusing on sound from a specific direction while reducing background noise [32]. More recently, deep learning has transformed source separation, enabling technologies such as music recognition systems that identify songs even in noisy environments [33], and AI-driven noise reduction in virtual meetings, which can intelligently distinguish speech from background interference in real-time [34].

The city soundscape problem provides an intuitive analogy for source separation in LISA data. Just as city streets are filled with overlapping sounds that blend into a complex auditory scene, LISA’s data stream is a cosmic symphony: gravitational waves from merging black holes and white-dwarf binaries overlap and mix with detector noise. Enter deep learning, which offers a data-driven approach to solving this astronomical puzzle. By utilizing robust architectures like convolutional and recurrent neural networks, deep-learning models can detect structured patterns hidden within the high-dimensional data, enabling scalable near-real-time blind source separation without prior knowledge of the number of sources [35, 36]. This paper marks the first step toward establishing deep source separation as a practical tool for LISA data analysis.

C. Contribution and overview of the paper

To address the challenge of source separation in LISA data, we introduce a deep learning-based framework designed to extract MBHBs, GBs, and instrumental glitches. Inspired by *demucs* (Deep extractor for music sources by Meta AI Research, see Ref. [37]), a model originally developed for the separation of musical instruments in audio data, our approach replaces the traditional sequential subtraction paradigm in LISA data analysis with single-step source extraction. By employing a shared encoder-decoder structure and latent space clustering, the model disentangles overlapping signals efficiently while remaining scalable to large source populations. A core feature of our framework is the frequency-binned output representation, which structures GB source separation on the basis of spectral content. This design helps mitigate source confusion by ensuring sources are dynamically clustered and disentangled in a learned feature space. Note that deep source separation operates independently of parameter estimation. This paper focuses on source separation, and parameter estimation based on its output is beyond the scope of this study.

The remainder of this paper is structured as follows. Section II provides an overview of the expected LISA dataset and signal characteristics, including the types of gravitational-wave sources and the impact of time-delay interferometry (TDI) on data representation. Section III describes our deep-learning framework, focusing on encoder-decoder architecture and latent space clustering. Section IV presents an evaluation of the model’s performance in extracting MBHBs, GBs, and glitches across various test scenarios. Finally, Section V presents conclusions and proposes future work, including potential extensions to more complex astrophysical scenarios, and integration with full-scale LISA data pipelines.

II. THE LISA DATASET

The dominant source populations in the millihertz LISA band are MBHBs and GBs, both of which present unique challenges for analyzing the LISA dataset. While MBHBs produce high-SNR transient signals, GBs form a persistent foreground that influences the detectability of other sources.

A. Massive black-hole binaries

MBHBs will be the loudest, most information-rich sources for LISA. They originate from the mergers of supermassive black holes at the centers of galaxies [38–40]. These systems are expected to be detected across cosmic history, with events observable up to redshifts of $z \approx 15$. Their gravitational-wave emission sweeps through the LISA band as the binary inspirals toward coalescence, producing a high-SNR signal that lasts hours to weeks,

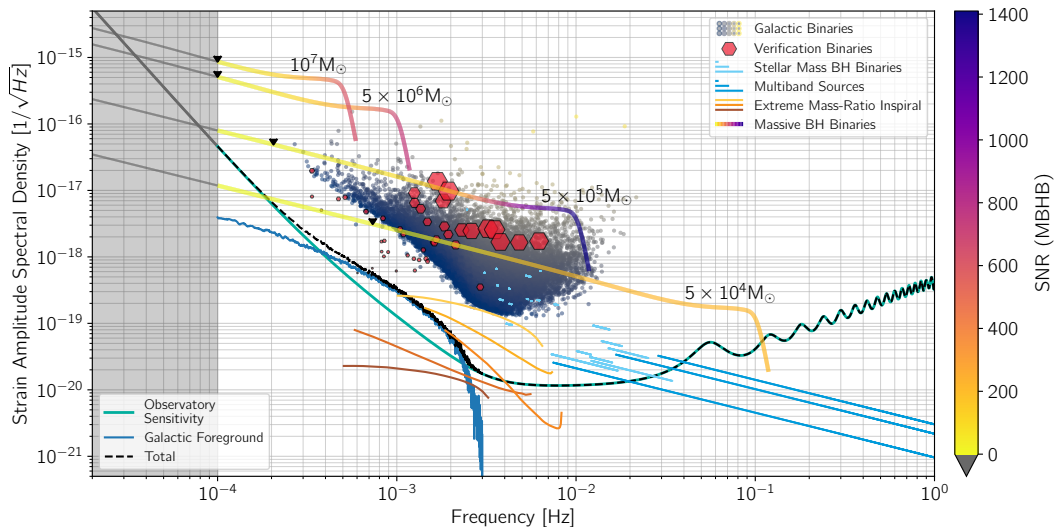


FIG. 1: Illustration of primary LISA source classes in the frequency-amplitude plane. It includes merging massive black-hole binaries and extreme mass-ratio inspirals at moderate redshift, stellar-mass black holes at low redshift, and Galactic binaries, with sensitivity limits shown for instrumental noise, the unresolved Galactic foreground, and their sum. The cloud of resolvable sources appears above the noise level due to the detection threshold being set at an SNR of 7. Reprinted from [1].

depending on the total mass and redshift. MBHB detections will provide critical insights into black hole formation, galaxy evolution, and accretion physics.

As illustrated in Fig. 1, MBHBs with total masses between 10^4 and $10^7 M_{\odot}$ lie well within the LISA band, making them some of the loudest and most distant signals in LISA. Lower-mass binaries spend more time in the LISA band before merging, whereas higher-mass systems transition through LISA’s frequency range more quickly. Some MBHBs may also be multiband sources, appearing first in LISA before merging within the detection range of ground-based observatories.

B. Galactic binaries

Compact binaries in the Milky Way, particularly double white-dwarf systems, are expected to dominate the LISA band between 0.1 mHz and 10 mHz, producing nearly monochromatic individual signals that persist throughout the mission [41–43]. Unlike MBHBs, these binaries evolve slowly, with minimal frequency drift over LISA’s observational timescale. A subset of these binaries will be individually resolvable, particularly those with higher SNRs and well constrained parameters from electromagnetic observations. These verification binaries, depicted as red hexagons in Fig. 1, may be considered calibration sources for LISA, having been pre-identified through optical and radio surveys. However, this characterization remains under debate [44]. The vast majority of GBs will be unresolved, forming a stochastic foreground noise that dominates the low-frequency LISA

band. This confusion-limited background, illustrated by the dashed black line in Fig. 1, limits LISA’s ability to detect fainter signals in the same frequency range, such as extreme mass-ratio inspirals (EMRIs) and a potential primordial gravitational-wave background.

C. Extreme mass-ratio inspirals

EMRIs are another important class of sources expected in the LISA band, resulting from the inspiral of a compact object – typically a stellar-mass black hole, neutron star, or white dwarf – into a much more massive black hole, usually found at the center of a galaxy [45–47]. These systems generate long-lived, complex waveforms as the smaller object undergoes tens of thousands of orbits before merging. EMRIs encode precise information about the spacetime geometry of the central massive black hole, making them key probes for testing strong-field General Relativity and the nature of black holes. EMRIs emit gravitational waves in the 1 mHz to 10 mHz range, overlapping with the Galactic foreground and some lower-mass MBHB signals. Their waveforms are highly intricate, containing multiple harmonics that encode information about the mass, spin, and orbital eccentricity of the system. Unlike MBHBs, which evolve rapidly through the LISA band, EMRIs remain in LISA’s sensitivity window for months to years, requiring long-duration signal tracking and advanced matched-filtering techniques. While EMRIs are a key LISA science target, they are not included in the dataset considered for this paper. The same applies to stellar-origin black-hole

binaries, and unmodeled gravitational wave bursts. Our focus is on MBHBs, GBs, and non-stationary noise artifacts. Future work needs to investigate incorporating these source types into deep source separation methods.

D. Instrumental noise and glitches

In addition to astrophysical sources, the LISA data stream will contain instrumental noise and transient artifacts, both of which impact signal extraction and parameter estimation. These noise sources arise from multiple factors, including laser frequency fluctuations, unmodeled spacecraft acceleration, optical measurement noise, and environmental disturbances affecting the stability of the interferometric measurements [48–50].

One significant challenge is the presence of non-stationary *glitches*, short-duration noise transients caused by spacecraft systematics or environmental perturbations, such as micrometeoroid impacts. These glitches can mimic or obscure real gravitational-wave signals, making their identification and mitigation essential for accurate source separation [51, 52]. Characterizing instrumental noise is an active area of study, and techniques such as machine learning-based anomaly detection may play a crucial role in distinguishing true astrophysical signals from noise artifacts [53].

E. Time-delay interferometry

Unlike ground-based detectors, which use simple Michelson interferometry, LISA’s evolving geometry introduces unique challenges in maintaining phase coherence, requiring an advanced signal-processing technique known as TDI [54–56]. TDI is designed to suppress laser frequency noise, which would otherwise overwhelm gravitational-wave signals. Laser noise suppression is accomplished by linearly combining and time-shifting LISA’s interferometric measurements to create virtual interferometers with equal arm lengths. It is important to note that the on-ground application of TDI transforms the data representation, altering the structure of signals compared to their raw strain measurements. For astrophysical data analysis, this transformation introduces additional complexity, since TDI modifies the apparent waveform morphology. In the context of machine learning, this requires that we train algorithms on TDI-processed data. Indeed, understanding these transformations is critical when designing traditional Bayesian inference or novel feature extraction methods.

III. FRAMEWORK FOR DEEP SOURCE SEPARATION OF LISA SIGNALS

The source separation framework presented in this paper is designed to extract astrophysical signals and to identify and estimate the evolution of glitches in the dataset. By taking advantage of the model’s ability to

learn structured latent representations, we can distinguish glitches from genuine gravitational wave events, reducing the risk of misclassification. This capability is particularly valuable in scenarios where glitches overlap with astrophysical signals, ensuring that transient artifacts do not interfere with the accurate reconstruction of MBHBs or GBs.

The following section provides an overview of key deep learning-based methods for source separation, highlighting their strengths and applications. This is followed by a detailed presentation of the framework developed in this work for LISA data analysis.

A. Overview of deep-learning techniques for source separation

A widely adopted approach in source separation involves *mask-based methods*, where neural networks are trained to estimate time-frequency masks that enhance the separation of individual sources when applied to the spectrogram of an input mixture [57, 58]. Typically, such architectures consist of a neural network that processes the magnitude spectrogram through layers of batch normalization, multiple bi-directional long short-term memory (BLSTM) networks, and a fully connected output layer with a sigmoid activation function to generate the masks. The network is trained using a reconstruction loss, commonly an L1 or L2 loss between the estimated and target spectrograms. Variations of mask-based methods include soft masking, where estimated masks take continuous values between 0 and 1, and hard masking, where values are binarized. This approach is particularly effective in speech separation and enhancement, as it leverages the structured nature of human speech signals.

Deep clustering presents an alternative approach, addressing source separation as an embedding-based learning problem [59–61]. Instead of estimating masks directly, deep clustering models learn to map each time-frequency bin of the input spectrogram into a high-dimensional embedding space. In this space, embeddings corresponding to the same source cluster together, while those from different sources remain well-separated. Clustering algorithms, such as *k*-means [62], are subsequently applied to assign time-frequency bins to their respective sources and generate separation masks. This method has shown superior performance in tasks such as blind source separation and reverberant speech separation, where the relationship between sources is highly nonlinear.

Chimera networks are hybrid architectures that integrate both mask-based and deep clustering techniques within a unified framework through multi-task learning [63–65]. These networks contain shared BLSTM layers, followed by dual output heads: one for deep clustering and another for mask inference. During training, the deep clustering objective serves as a regularizer, enhancing the generalization capability of the network, while

the mask inference objective is used for direct source separation during inference. Chimera networks have demonstrated improved robustness in real-world conditions, benefiting from the complementary strengths of both deep clustering and mask-based learning.

While source separation traditionally operates on spectrogram representations, time-domain approaches have emerged as a powerful alternative, enabling direct processing of raw audio waveforms [66, 67]. Time-domain models have demonstrated state-of-the-art performance, surpassing traditional spectrogram-based approaches in many benchmarks due to their ability to preserve phase information and reduce artifacts introduced by spectral transformations. Notable architectures in this category include Conv-TasNet [68], a convolutional time-domain audio separation network that employs an encoder-decoder structure with temporal convolutional networks. By replacing the conventional short-time Fourier transform with a learned encoder, Conv-TasNet captures fine-grained temporal structures, enhancing speech separation quality. Another prominent model, **demucs** [37], is inspired by deep generative models for audio and features a U-Net-like architecture [69] with a convolutional encoder, a BLSTM-based bottleneck and a decoder utilizing transposed convolutions. This design effectively captures both local and long-range temporal dependencies, making **demucs** particularly well-suited for music source separation tasks, where harmonic and percussive elements are intertwined. In this work, we employ a modified **demucs**-based encoder-decoder network. We outline its mathematical theory in the next section.

B. Encoder-decoder architectures

In this paper, deep learning-based source separation employs an encoder-decoder architecture, encoding raw input signals into a compressed latent representation before reconstructing the individual components. Unlike spectrogram-based methods, time-domain approaches naturally preserve phase information and reduce spectral artifacts, which is important for signal reconstruction in high-dimensional gravitational wave data. In the context of LISA, the encoder processes a noisy mixture and extracts the most important patterns and features, transforming the raw input into a more structured form. At the core of this process is the *bottleneck*, a stage where information is temporarily compressed, ensuring that only the most relevant details are retained while filtering out noise and redundancies. The bottleneck representation helps the model focus on essential aspects of the data, improving the separation of different sources. Finally, the decoder uses this refined information to reconstruct the individual signals corresponding to MBHBs, GBs, and glitches. This section introduces the mathematical foundations behind this framework and explains how it helps disentangle overlapping signals effectively.

1. Encoder

The shared encoder is responsible for mapping raw LISA TDI data into a structured latent space that highlights key features relevant to source separation. The term “shared” refers to the fact that a single encoder processes the entire input mixture and extracts a common feature representation, which is then used by multiple decoders to reconstruct individual sources. Instead of training separate encoders for each source type, a shared encoder ensures unified feature extraction, improving efficiency and consistency in learned representations.

Given a raw time-domain signal $x(t)$, the encoder function can be formulated as

$$z = E(x; \theta_E), \quad (1)$$

where z represents the latent space encoding that captures essential waveform structures, while $E(\cdot; \theta_E)$ denotes the encoder network parameterized by θ_E . The encoder typically comprises multiple convolutional layers to extract local time-frequency patterns, followed by nonlinear activations to improve source separability. The parameters θ_E are learned through training.

2. Latent representation and bottleneck transformation

The latent space provides a compact representation of extracted features, facilitating the separation of individual sources. In the context of blind source separation, it enables the mapping of overlapping signals to distinct regions, aiding in their disentanglement and improving reconstruction accuracy. The transformation reduces redundancy, ensuring that the model focuses on independent components. To further refine the extracted features and prevent the network from overfitting, an additional constraint is introduced through the bottleneck layer. The bottleneck layer serves as a regularization mechanism, limiting the amount of information passing through the network. It ensures that only the most relevant features are retained while suppressing noise and redundant details. This process can be expressed as

$$\tilde{z} = g(z; \theta_B), \quad (2)$$

where \tilde{z} represents the bottleneck encoding, $g(\cdot; \theta_B)$ is the low-dimensional projection that filters irrelevant components while preserving key signal characteristics required for reconstruction and θ_B represents the trainable parameters of the bottleneck function.

A more rigorous way to understand the bottleneck transformation is through information theory, where the goal is to find a representation \tilde{z} that retains as much relevant information about the original signal $x(t)$ as possible while discarding unnecessary details (e.g., noise and redundant components). This is captured by the *information bottleneck objective* [70], which aims to optimize

the trade-off between compression and preservation of useful information:

$$\max_{\theta_B} I(\tilde{z}; x) - \beta I(\tilde{z}; n). \quad (3)$$

Here, $I(A; B)$ represents the mutual information between two variables, quantifying how much knowing one reduces uncertainty about the other. The term $I(\tilde{z}; x)$ ensures that the compressed representation \tilde{z} still retains meaningful information about the input. The term $I(\tilde{z}; n)$ represents the amount of irrelevant information (such as noise) that the bottleneck still encodes. The Lagrange multiplier β controls the balance: a higher β enforces stronger compression, forcing the network to discard more information. By optimizing Eq. 3 over the bottleneck parameters θ_B , the model learns to remove redundancy while keeping only the most essential features, improving the separation of signals.

3. Decoder

The decoder reconstructs individual sources from the shared latent space by applying learned transformations. Each decoder head receives the same latent input but is trained to reconstruct only a specific target source:

$$\hat{x}_i = D_i(\tilde{z}; \theta_{D_i}), \quad (4)$$

where \hat{x}_i is the reconstructed output for the i -th source, and $D_i(\cdot; \theta_{D_i})$ represents the decoder network parameterized by θ_{D_i} , responsible for reconstructing individual components. The decoder can apply a series of transposed convolutions to progressively upsample and restore temporal structures from the compressed latent representation. To enhance reconstruction accuracy, *skip connections* can be incorporated, allowing the network to retain fine-grained details by reintroducing relevant features from earlier encoding layers. Typically, source-specific activation functions are employed to ensure that each decoder head reconstructs only its assigned target, preventing interference between different signal types.

C. Demucs as an example of an established encoder-decoder model

After introducing the fundamental principles of encoder-decoder architectures and latent space representations, we now turn our attention to **demucs**. The model has demonstrated success in audio source separation tasks and will be adapted for gravitational wave data analysis in the context of LISA.

Unlike spectrogram-based approaches that rely on time-frequency representations, **demucs** operates directly on raw audio waveforms, allowing the model to fully leverage the temporal and structural characteristics of

sound, resulting in improved separation performance [37]. At its core, **demucs** is based on a U-Net convolutional architecture. U-Net consists of an encoder-decoder framework with symmetric skip connections that link corresponding layers between the encoder and decoder paths [71]. Note that skip connections mitigate the bottleneck’s impact by reintroducing high-resolution features. In **demucs**, where maintaining the temporal structure of waveforms is essential, these connections help preserve fine details that might otherwise be lost during compression.

The encoder in **demucs** comprises multiple convolutional layers that progressively downsample the input, capturing hierarchical features. Each convolutional block integrates standard convolutions, batch normalization, and nonlinear activation functions to enhance feature extraction. To further improve its capacity to model long-range temporal dependencies, **demucs** incorporates BLSTM layers within the bottleneck, allowing the model to process both forward and backward temporal information. This feature is particularly advantageous for disentangling overlapping musical components, which frequently exhibit strong temporal correlations. Additionally, **demucs** employs gated linear units as activation functions, which enhance the model’s expressiveness by selectively regulating information flow.

The decoder path in **demucs** employs transposed convolutional layers to upsample the encoded features, reconstructing the separated sources while preserving their fine-grained temporal structure. The inclusion of skip connections from the encoder to the decoder ensures that high-resolution details lost during downsampling are retained, leading to accurate reconstruction of the separated signals.

Demucs integrates several additional techniques to improve performance. Its multi-scale processing capability, facilitated by the hierarchical convolutional structure, enables the model to capture both short-term transients and long-term harmonic structures. Although **demucs** is trained on short audio snippets, it can process long audio sequences effectively by incorporating *overlapping window inference*. This approach involves applying a sliding window with overlapping segments, which not only mitigates boundary artifacts but also ensures smooth transitions between separated chunks, thereby preserving temporal consistency over extended durations.

D. Modifying demucs for application in LISA

Adapting **demucs** for LISA data requires modifications that account for the unique characteristics of gravitational-wave signals. Unlike conventional audio streams, LISA data comprises a superposition of overlapping astrophysical waveforms and transient instrumental glitches. The primary challenge in this adaptation lies in accurately isolating individual sources while ensuring the scalability of the separation model. To address this, we

design a modified architecture to structure the separation task across three dedicated decoder heads following a shared encoder and bottleneck representation. The first decoder is responsible for reconstructing MBHB signals, assuming for simplicity that individual MBHB events do not overlap in time. The second decoder isolates non-stationary noise artifacts, such as transient glitches. The third decoder is specifically designed for GBs and consists of multiple output channels, each corresponding to a pre-defined frequency bin. This multi-output design enables the model to disentangle individual GB sources while maintaining scalability. Instead of assigning a separate decoder to each GB source – an approach that quickly becomes computationally prohibitive – the frequency space is discretized into small bins, ensuring that each bin contains at most one dominant source. In our framework, we intentionally omit skip connections to maintain simplicity. As a result, our bottleneck applies a weaker compression compared to *demucs*. Details will follow.

We use LISA’s TDI data streams A, E, and T [72] as input to the model. For now, each TDI channel is processed independently, applying the same separation model. An extended version of the framework could allow multiple TDI streams to be processed in parallel. This extension might further optimize source separation accuracy by taking advantage of complementary information from different TDI observables during training and inference, but it is not required for this demonstration. The schematic architecture of the *demucs*-inspired multi-source extraction model is depicted in Fig. 2.

1. Encoder and bottleneck architecture of LISA-modified *demucs*

The encoding process transforms the noisy TDI time series containing overlapping MBHBs, GBs, and glitches into a structured latent representation. The encoder consists of four consecutive one-dimensional convolutional layers with increasing feature dimensions, each followed by a ReLU activation to introduce nonlinearity. This hierarchical feature extraction progressively captures waveform structures at different resolutions, preserving temporal patterns. Once the latent representation z is obtained, a bottleneck layer refines the extracted features by applying an additional one-dimensional convolution. Here, the bottleneck transformation restructures the learned representations by reducing the number of feature channels rather than compressing the sequence length. The encoder follows a shared architecture, utilizing a single feature extraction pipeline for all sources. Table I summarizes the network configuration.

Since the first three convolutional layers in the encoder apply a stride of 2 each, the input time series is progressively downsampled by a factor of $2^3 = 8$, meaning the sequence length is reduced to 1/8 of the original input. Note that the bottleneck layer does not further compress the sequence length because it applies a con-

TABLE I: Encoder and bottleneck network configuration. The padding parameters are chosen to ensure that, when combined with the decoder, the framework’s outputs match the dimension of the input signal.

Layer	Input	Output	Kernel	Stride	Padding
Conv1D	1	64	8	2	3
ReLU	-	-	-	-	-
Conv1D	64	128	8	2	3
ReLU	-	-	-	-	-
Conv1D	128	256	8	2	3
ReLU	-	-	-	-	-
Conv1D	256	512	8	1	4
ReLU	-	-	-	-	-
Bottleneck	512	256	3	1	1

volution with stride 1. Instead, it reduces the number of feature channels from 512 to 256, serving as a feature refinement step rather than a strict compression bottleneck. Unlike *demucs*, which uses skip connections to preserve fine-grained details, our encoder does not include skip connections for now. Therefore, we decided that the bottleneck layer should preserve the temporal resolution while focusing on channel-wise dimensionality reduction. In future work, we plan to experiment with the combination of skip connections and bottleneck compression to assess their impact on feature retention and downstream tasks.

In Section IV, we will visualize the bottleneck-encoded latent features using t -distributed stochastic neighbor embedding (t -SNE) [73], a dimensionality reduction technique that maps high-dimensional data into a lower-dimensional space to illustrate the clustering patterns in typical LISA TDI data.

2. Multi-source decoder heads for MBHBs, GBs, and glitches

The decoder reconstructs individual gravitational-wave signals from the shared latent representation by applying a dedicated decoding process for each source type. It follows a transposed convolutional architecture similar to *demucs*, where the extracted latent features are progressively upsampled back into de-noised time-domain waveforms. Each decoder consists of three transposed convolution layers with ReLU activations, allowing for structured reconstruction of the signals.

For MBHB and glitch signals, the decoder reconstructs the time-domain waveform as a single-channel output. This design choice assumes for simplicity that MBHB merger signals occur at sufficiently distinct times, eliminating the need for explicit separation. Additionally, instead of resolving individual glitches, the model treats them as a collective class and outputs a single data stream that may contain multiple glitches.

For GB sources, we adopt a different approach. The decoder utilizes a frequency-binned method, generating a

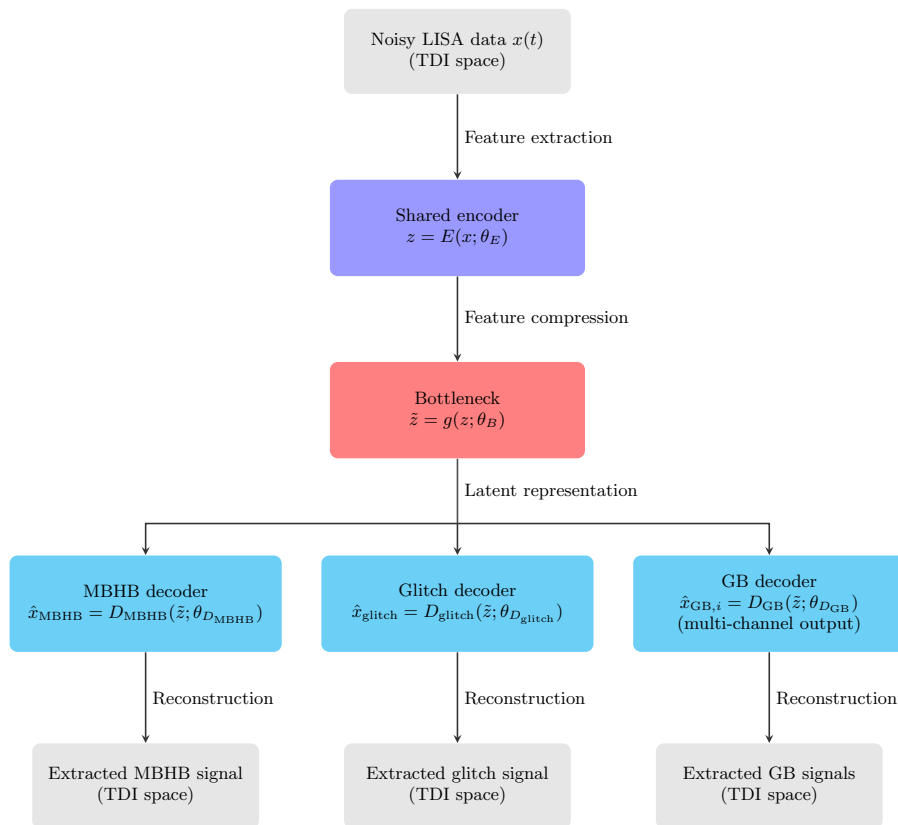


FIG. 2: Deep source separation framework for LISA data, where a shared encoder compresses the TDI input, and decoders reconstruct MBHBs, GBs and glitches. Since the input data denotes a TDI channel, the separated and decoded output signals are represented in the TDI space, as well.

multi-channel waveform where each channel corresponds to a distinct frequency bin. Each bin reconstructs the portion of the GB compound that falls within its designated frequency range. This design eliminates source permutation ambiguity and allows the model to accommodate an arbitrary number of GB sources efficiently. The implementation features a final transposed convolution layer with N_{GB} output channels, where N_{GB} denotes the predefined number of frequency bins. The decoder processes the latent representation in a single forward pass, simultaneously producing a time-domain waveform for each bin. If a bin contains no GB sources, the model naturally learns to suppress that output channel.

Table II summarizes the architecture of the decoder networks used for reconstructing MBHB, GB, and glitch waveforms. Note that the padding parameters are selected to ensure that the decoded signals retain the same length as the input signal prior to encoding.

Each decoder (MBHB, glitch, and GB) follows this same transposed convolutional architecture, upsampling the latent representation back to the time-domain waveform. The structure ensures that the output sequence length matches the original input length after three layers of transposed convolution with stride 2. This preserves the temporal coherence of the reconstructed signals. By

TABLE II: Decoder network configuration. The output channel dimension c is 1 for MBHBs and glitches, while it is set to N_{GB} for GBs, where each channel corresponds to a frequency bin. Note that ConvTranspose1D performs the inverse operation of Conv1D.

Layer	Input	Output	Kernel	Stride	Padding
ConvTranspose1D	256	128	8	2	3
ReLU	-	-	-	-	-
ConvTranspose1D	128	64	8	2	3
ReLU	-	-	-	-	-
ConvTranspose1D	64	c	8	2	$4+1^a$

^a An additional output padding of 1 is applied to ensure the decoded signals match the input signal length, which is required for computing the loss function.

using a frequency-binned approach for GB separation, the model effectively assigns sources to their nearest bin based on frequency content. This strategy eliminates the need for a predefined number of GB sources and ensures scalability to thousands of sources.

In the simulation section of this paper, we will use a low value for N_{GB} and explore more realistic populations in a future study by increasing the number of hidden layers, neurons, and training data size.

3. Loss calculation and training

The model is trained by optimizing a total loss function that consists of individual Mean Squared Error (MSE) loss terms for MBHBs, GBs, and glitches. The loss is computed based on the reconstructed waveforms produced by the decoder and their corresponding ground truth signals. The total loss function is defined as

$$L_{\text{Total}} = L_{\text{MBHB}} + L_{\text{GB}} + L_{\text{glitch}}, \quad (5)$$

where L_{MBHB} , L_{GB} , and L_{glitch} represent the reconstruction losses for each source type.

For MBHB and glitch signals, the loss is computed directly by comparing the predicted output \hat{x} with the ground truth x using MSE:

$$L_{\text{MBHB}} = \text{MSELoss}(\hat{x}_{\text{MBHB}}, x_{\text{MBHB}}) \quad (6)$$

and

$$L_{\text{glitch}} = \text{MSELoss}(\hat{x}_{\text{glitch}}, x_{\text{glitch}}). \quad (7)$$

For GB sources, a frequency-binned representation is used to ensure structured separation of the overlapping signals in the spectral domain. We map the GB signals into discrete frequency bins using a bin assignment function, which finds the nearest predefined frequency bin for each GB signal in the data and accumulates its contribution into the corresponding bin. Formally, for a batch of GB signals x_{GB} with associated frequencies f_{GB} , the binned representation is given by:

$$x_{\text{GB}}^{\text{bin}}[b, b_i] = \sum_i x_{\text{GB}}[b, i]$$

with $b_i = \text{arg min } |f_{\text{GB},i} - f_{\text{bins}}|$

where b represents the batch index, b_i is the index of the closest frequency bin for source i , and f_{bins} is a predefined list of frequency bin edges used to categorize GB signals based on their frequencies. The frequency-binned ground truth signal is then compared to the predicted GB output using MSE:

$$L_{\text{GB}} = \text{MSELoss}(\hat{x}_{\text{GB}}, x_{\text{GB}}^{\text{bin}}). \quad (8)$$

For this strategy to resolve each GB individually, the bin width must be small enough to ensure that each bin contains at most one GB source. If the bins are too large, multiple sources will be mapped to the same bin, leading to signal blending. Conversely, if there are fewer GB sources than bins, the model suppresses the corresponding outputs, maintaining efficiency while ensuring scalability to thousands of sources without requiring prior knowledge of the actual number of GB signals in the data.

After computing the total loss, gradients are propagated backward through the network, and model parameters are updated using the Adam optimizer. The optimization process follows standard backpropagation, iteratively refining the trainable parameters of the encoder,

bottleneck, and decoder networks. The training loop follows these key steps:

1. The model receives mixed gravitational-wave signals as input and predicts the MBHB, glitch, and GB outputs.
2. The loss is computed separately for MBHBs, glitches, and frequency-binned GBs.
3. The gradients are computed using backpropagation, and model parameters are updated using the Adam optimizer.
4. The process is repeated for multiple training epochs, progressively improving the model's ability to disentangle overlapping signals.

Given that LISA observations span months to years, the model must handle long-duration signals while maintaining source coherence. Training on full-time-series data is computationally infeasible, so the model is trained on short-duration snippets analogously to the approach followed in `demucs`. During inference, overlapping segments are processed independently, and efforts are currently underway to develop and refine a method for seamlessly merging these segments using a weighted averaging scheme. This work will be presented in a follow-up paper.

Note that the original `demucs` architecture is more complex than the implementation used in this study. It features a deeper network structure with additional convolutional layers, a larger number of feature channels, and BLSTM layers to model long-range dependencies in audio waveforms. In contrast, our implementation adopts a simplified architecture with fewer layers and reduced model complexity, focusing primarily on demonstrating the feasibility of deep blind source separation in LISA's TDI data. While we currently maintain this streamlined model for proof-of-concept simulations, it is possible to further converge toward the full `demucs` architecture by increasing network depth, adding additional hidden layers, or expanding the number of neurons in each processing stage. The flexibility of the chosen framework ensures that extensions are feasible, enabling the method to be progressively adapted for larger and more intricate LISA data analysis tasks. As the scope of this study is not to resolve the full source population expected in LISA but rather to demonstrate the viability of deep learning-based source separation in a controlled setting with a limited number of sources, we stick to the architectural design proposed in this section when presenting the simulation results in the following. The simplified design already proves effective in achieving remarkable separation of individual signals, suggesting that deep learning-based source separation can offer a more streamlined approach to future pipeline implementation.

IV. SIMULATION RESULTS

The section presents the results of the trained multi-source separation model applied to simulated TDI data. We first describe the characteristics of the training dataset, including the astrophysical and instrumental components used to construct the input mixtures. We then examine the learned latent space representation, providing insight into how the shared encoder organizes different source types. Finally, the model’s performance is evaluated across a range of test scenarios, demonstrating its ability to extract overlapping sources, reconstruct weak signals, and handle realistic noise conditions.

A. Training data and simulation setup

The training dataset consists of simulated LISA TDI time series, incorporating a superposition of merging MBHBs, GBs, transient glitches, and stationary instrumental noise. The data is generated using the `BBHx` package for MBHBs [74–76] and `FastGB` for GBs [77], ensuring physically motivated waveforms. Each time series is sampled at a rate of $\Delta t = 5$ seconds, with individual training snippets lasting for 2 hours.

The MBHB waveforms span a mass range of $10^5 M_\odot$ to $10^6 M_\odot$ per binary component, distributed across redshifts from $z = 2$ to $z = 5$. These sources are modeled using spin-aligned inspiral-merger-ringdown waveforms with higher-order harmonic modes, simulating the final inspiral phase visible to LISA. GBs are generated from a population of compact white-dwarf binaries, covering frequencies between 1 mHz and 10 mHz. In this proof-of-concept study, the individual GB strains are considered to lie within the range of 1×10^{-22} to 2×10^{-21} . We assume an upper limit of $N_{\text{GB}} = 5$ GBs, indicating that each dataset may include up to five time-overlapping GB sources in addition to MBHBs and glitches. However, the actual number could be lower, remains unknown a priori, and must be inferred by the model. Scaling to realistic GB populations is underway and will be the subject of future publications. The instrumental noise follows the expected LISA sensitivity curve, while transient glitches are drawn from a randomized distribution to reflect possible instrumental artifacts.

We train the model with a fixed learning rate of 10^{-3} , the Adam optimizer, and the loss function of Eq. 5. Training is performed for 25 epochs with a batch size of 16, ensuring convergence across all decoder heads. The training dataset comprises 25,000 different data samples.

Figure 3 presents a representative training sample, highlighting the interplay of MBHBs, GBs, glitches, and noise in the top panel, with the individual components displayed below. To start, the glitch distribution here is relatively simple. We will present more complex signal-artifact overlaps and glitch patterns throughout this section.

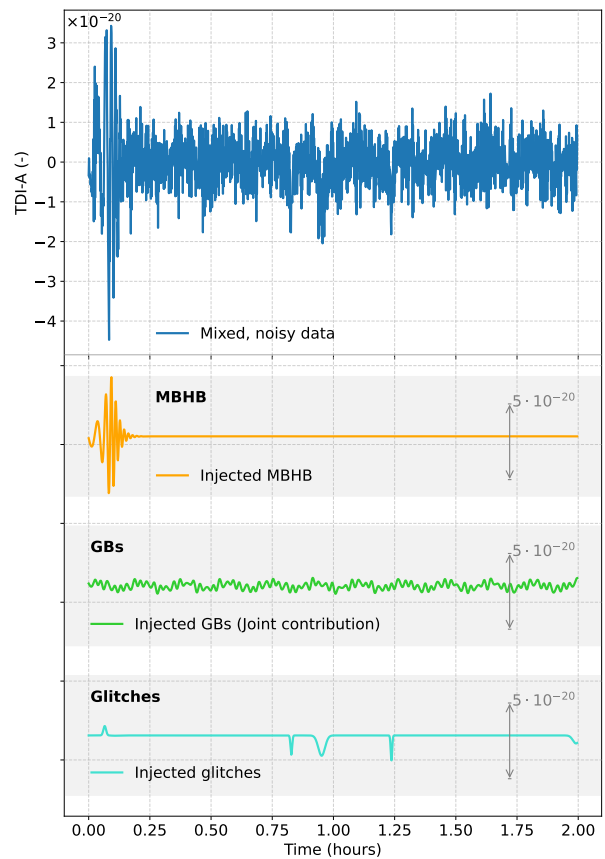


FIG. 3: Example of a time-domain representation of LISA’s TDI data, capturing contributions from a merging MBHB, GBs, glitches, and stationary noise, used for model training and testing. The upper panel presents the noisy TDI-A channel, while the lower panels decompose it into individual signal components, which the proposed framework seeks to separate. Note that in this evaluation, we display solely the second-generation TDI-A channel, excluding the E and T observables.

B. Latent space representation

To analyze the structure of the learned latent representation, we extract and visualize the bottleneck-encoded features from the trained model. This visualization provides insight into how different signal components are represented in the latent space. Figure 4 displays the two-dimensional t -SNE projection of the latent representations obtained from the encoded features of the time series in Fig. 3. Each component – MBHB, GBs, and glitches – is processed separately through the trained encoder and bottleneck layer, producing latent space representations of shape $(256, 180)$, where 256 corresponds to the number of feature channels, and 180 represents the compressed temporal dimension. Before applying t -SNE, these latent features are reshaped and standardized using z -score normalization. Specifically, we concatenate

the latent representations across the three signal types into a single dataset, ensuring that all features are on a comparable scale. We use the t -SNE algorithm [73] with a perplexity of 15. The perplexity parameter in t -SNE controls the balance between local and global structure in the projection. Lower perplexity values emphasize local structure, while higher values capture more global relationships. Each time step from the bottleneck layer is visualized as an individual data point in the scatter plot, color-coded by its corresponding source category.

The t -SNE projection reveals distinct clustering patterns associated with different signal components, indicating a degree of structure in the learned latent space. While t -SNE is a non-linear method that does not guarantee to preserve global distances, its ability to highlight local relationships allows us to identify grouping tendencies within the latent space. For instance, the MBHB (orange) and GB (green) components display distinct ring-like structures. While these patterns may be partially influenced by the *crowding problem*, where high-dimensional data is compressed into a lower-dimensional representation, their presence suggests that the model has learned to encode different signal types in a structured manner. Such clustering behavior, even if influenced by the properties of t -SNE, reflects an underlying organization in the learned representations.

Glitches (turquoise) appear more dispersed, forming multiple clusters with some points scattered throughout the latent space. This dispersion may indicate challenges in encoding glitches into a single representation but could also reflect a genuine structural variation in the data. Some overlap between glitch and astrophysical signal clusters suggests possible feature entanglement, which may be mitigated through further refinements to the model architecture or loss function.

Overall, the observed clustering in the t -SNE projection supports the idea that the model has captured structured representations of the data. While t -SNE does not provide definitive proof of disentanglement due to its tendency to distort global relationships, it offers valuable insight into the organization of latent features. To further validate the model’s representation learning, complementary dimensionality reduction techniques such as Principal Component Analysis (PCA) [78] or Uniform Manifold Approximation and Projection for Dimension Reduction (UMAP) [79] could be applied. A more rigorous evaluation, namely direct signal reconstruction quality, is performed in the following to confirm that the representation of TDI data in a latent space is indeed useful for our practical application.

C. Model evaluation on unseen test data

To evaluate the model’s generalization capability, we apply it to unseen test data and compare its predictions to ground-truth signals.

Figure 5 shows the reconstructed MBHBs, GBs, and

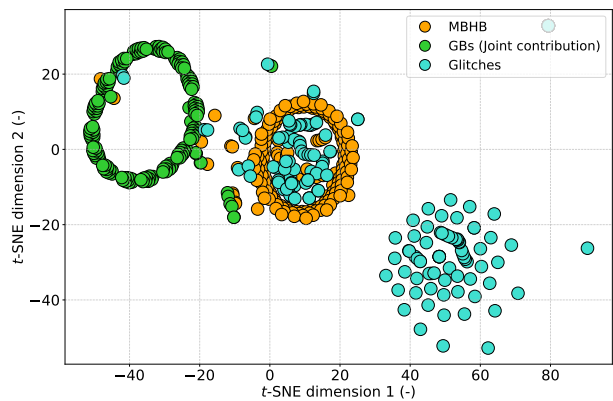


FIG. 4: t -SNE projection of bottleneck-encoded features derived from the normalized time series data in Fig. 3, illustrating clustering of merging MBHBs, GBs, and glitches. Note that separating sources within an abstract feature space beyond traditional temporal and spectral domains denotes a reorientation of methodology in LISA data analysis.

glitches of Fig. 3 obtained by the decoder heads and the bottleneck features visualized in Fig. 4. The upper panel illustrates the signal mixture, which serves as the input for our framework. The lower panels display the contributions separated for clarity, where the injected waveforms are compared with the corresponding estimates obtained with the deep source separation approach.

To validate the quality of the learned encoder-decoder framework, we use the absolute normalized match factor, which quantifies the similarity between a predicted waveform \hat{x} and a true waveform x on TDI level. The metric is defined as

$$M = \frac{|\langle x|\hat{x} \rangle|}{\sqrt{\langle x|x \rangle \langle \hat{x}|\hat{x} \rangle}}, \quad (9)$$

where the inner product $\langle x|\hat{x} \rangle$ is weighted by the noise power spectral density $S_n^X(f)$ in a given TDI channel:

$$\langle x|\hat{x} \rangle = \sum_f \frac{X(f)\hat{X}^*(f)}{S_n^X(f)}. \quad (10)$$

Here, $X(f)$ and $\hat{X}(f)$ are the Fourier transforms of x and \hat{x} , respectively.

The decoders accurately recover the merging MBHB, glitches, and GBs signals for this simple example. Regarding the multi-output channel GB decoder, we present only the prediction of the joint GB contribution obtained by summing all individual GB predictions. An analysis of the individually resolved GB sources follows at the end of this section. We further examine the model’s robustness by analyzing specific test cases that challenge its separation ability. These scenarios include strong overlaps between glitches and MBHBs, weak MBHB signals buried in noise, quiet periods without MBHBs, and high-density GB regions.

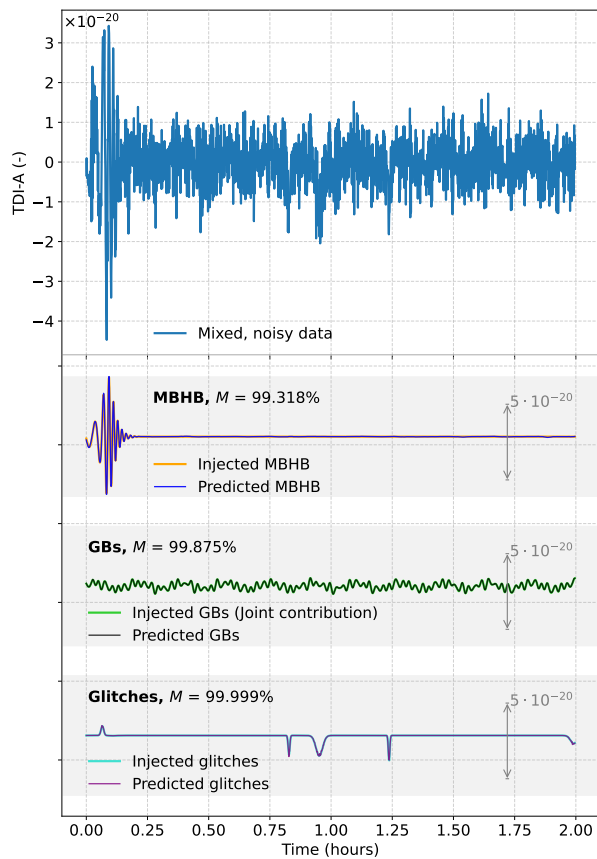


FIG. 5: Time-domain predicted waveforms from the deep source separation model overlaid on the true waveforms from Fig. 3, illustrating the model’s ability to accurately disentangle, reconstruct, and de-noise individual components.

1. Glitches overlapping with MBHB signal

A critical challenge in LISA data analysis is distinguishing instrumental glitches from astrophysical sources. To test the model’s performance in such cases, we consider examples where glitches overlap with MBHB waveforms during their inspiral, merger, and ringdown phases. Figure 6 compares the raw input signal, the true waveforms, and the model’s predicted outputs in such scenarios.

2. Weak MBHB mergers buried in noise

Another important test is the model’s ability to extract weak MBHB signals from the noise floor. In this scenario, the MBHB is barely visible in the input time series, simulating the detection of high-redshift mergers. Figure 7 presents two examples: one where the model successfully recovers the MBHB waveform, albeit with some power leakage into the glitch decoder, and another where it fails as the merger amplitude is further reduced.

3. Quiet periods with no MBHB mergers

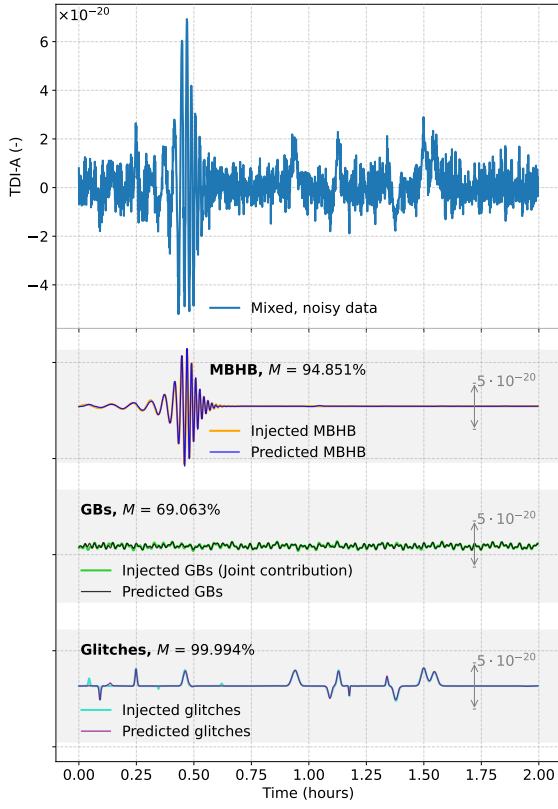
An essential test for avoiding false positives is evaluating the model in time periods where no MBHB is present. Figure 8 shows an input segment containing only GBs and stationary noise. The MBHB decoder output remains close to zero, indicating that the model does not hallucinate signals when none are present.

4. Resolving individual GBs in the presence of MBHBs and glitches

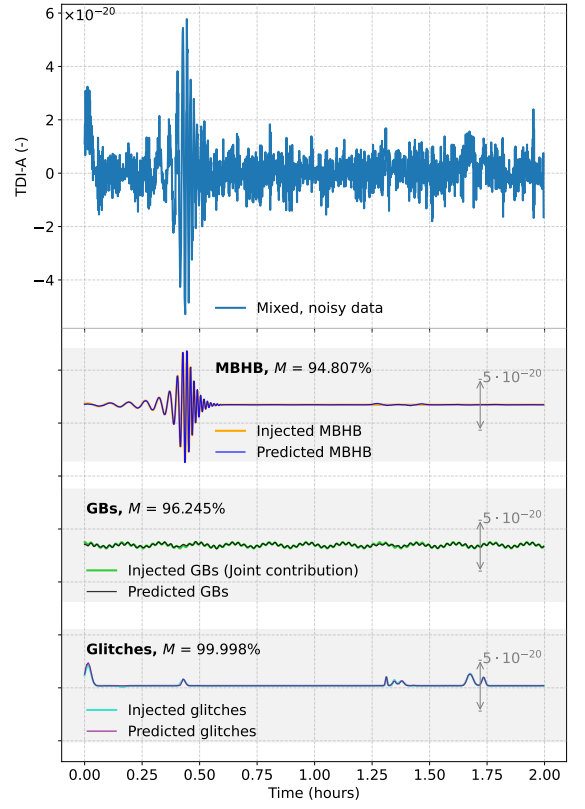
Finally, we evaluate the performance of the GB decoder in distinguishing individual and overlapping GBs. Figures 9 and 10 compare the true and predicted number of GBs, demonstrating that the model accurately estimates the number of active sources even in the presence of glitches and merging MBHB. This supports the effectiveness of the frequency-bin approach. We notice that the outputs of silent channels are not entirely zero. This is expected, given the decoder design. In future iterations, we plan to refine the GB decoder head by incorporating a gating mechanism that learns to fully suppress inactive channels, minimizing spurious noise when no signal is present in a given bin.

Scaling to the thousands of overlapping GBs anticipated in LISA’s observations will require a more complex network architecture and larger training datasets. Additionally, integrating a multi-resolution transform, such as wavelets, into the encoder design may be essential. However, even with these enhancements, a decrease in GB separation performance is expected when analyzing realistic populations on small datasets. The expected decrease in resolution performance stems from the inherent challenges in resolving individual GB signals within a densely populated frequency spectrum. In the LISA frequency band, millions of GBs are expected to emit gravitational waves, leading to overlapping signals that create a confusion noise. This overlap makes it difficult to distinguish individual sources. Traditional methods for GB parameter estimation face similar issues, as they rely on resolving individual signals from a complex superposition of numerous sources. Consequently, longer observation times are necessary to improve the signal-to-noise ratio and to accurately infer waveform parameters.

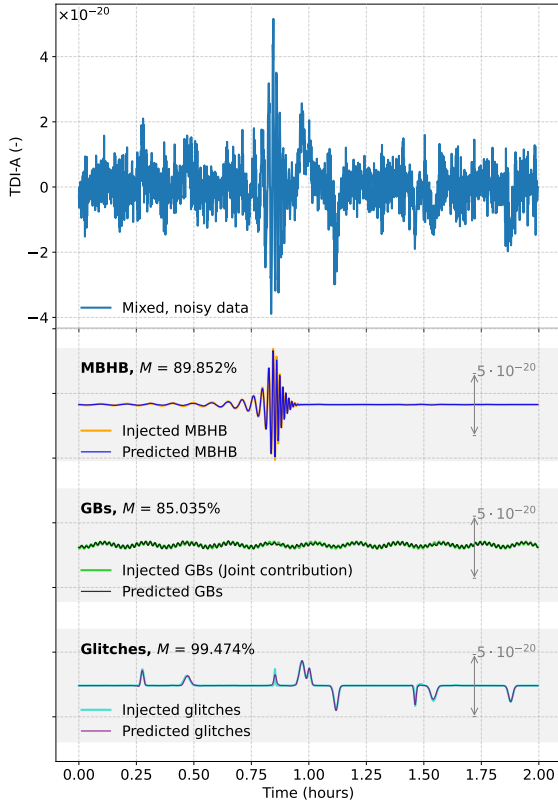
From this perspective, our model is designed with scalability in mind; we train on short data snippets and plan to apply a Demucs-like stitching procedure in future work to process arbitrarily long datasets once the model is trained. This approach involves segmenting long data streams into manageable, overlapping pieces, processing each segment individually, and then combining the results to reconstruct the full signal. This method has been effective in demucs and shows promise for application in gravitational wave data analysis. However, it’s important to note that this stitching procedure is not part of the current study and will be explored in a follow-up investigation.



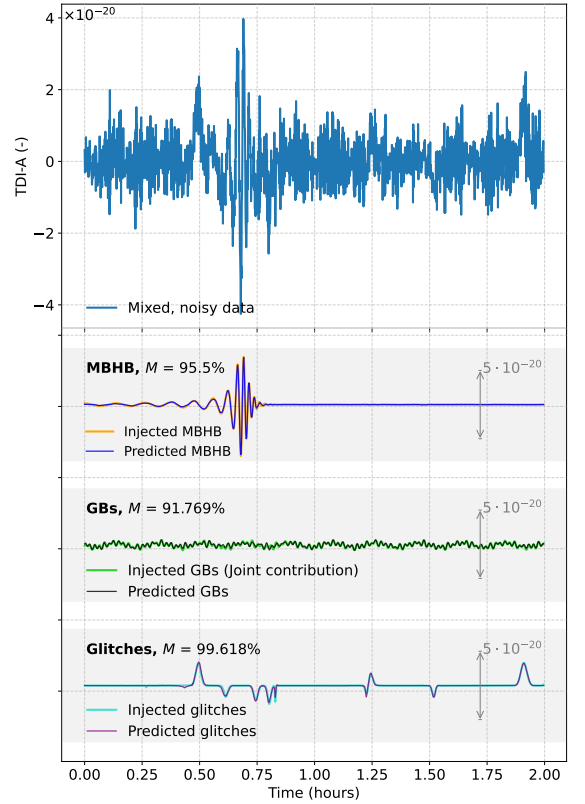
(a)



(b)



(c)



(d)

FIG. 6: Injected waveforms and model predictions in the presence of overlapping instrumental glitches. Panels (a) and (b) show cases where glitches overlap with the MBHB merger phase, while (c) and (d) illustrate glitches occurring during the MBHB ringdown.

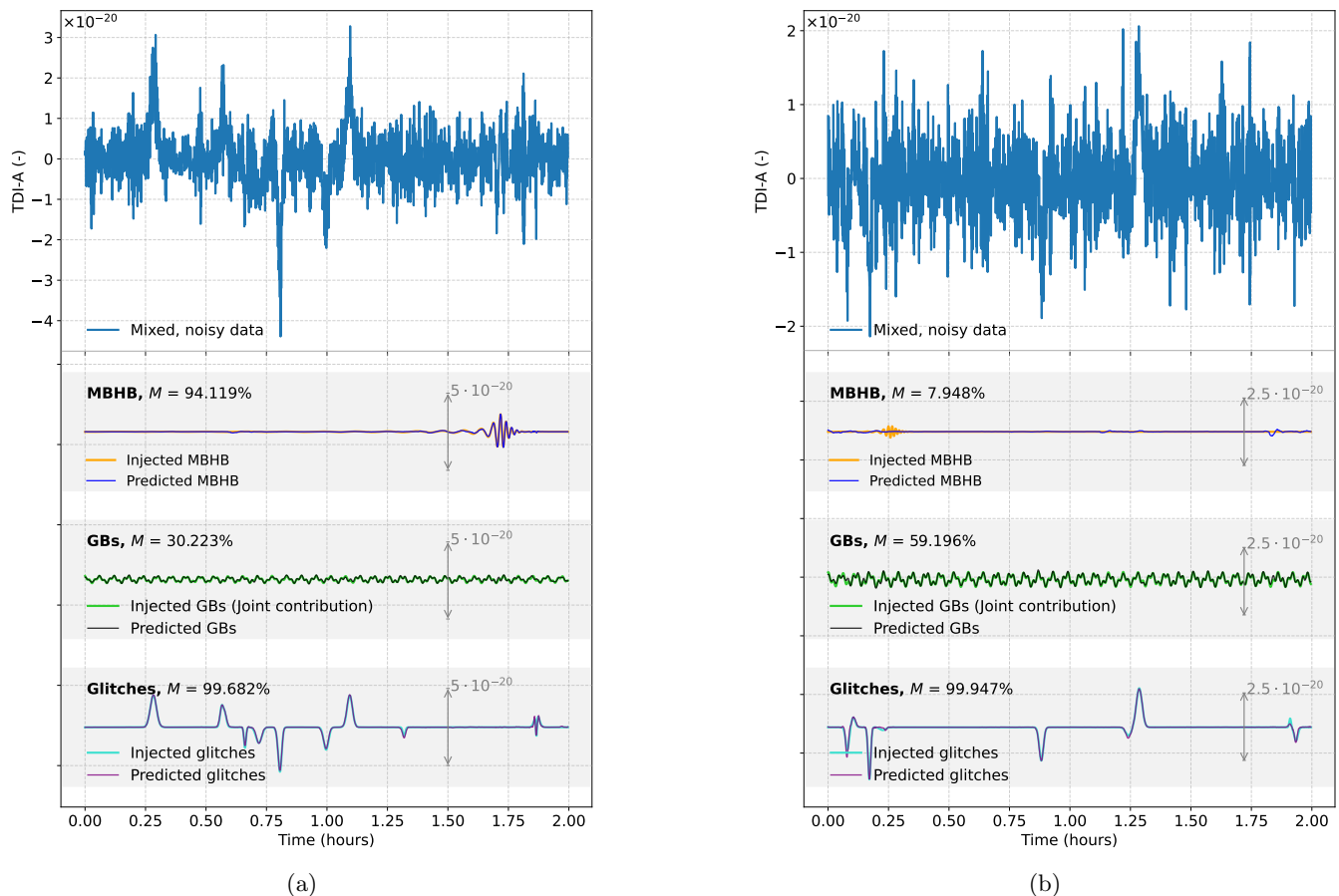


FIG. 7: Comparison of injected waveforms and model predictions for a low-amplitude MBHB merger buried in stationary noise. In panel (a), the deep source separation framework successfully detects and reconstructs the MBHB signal. However, in (b), where the signal amplitude is further diminished, the model fails. In such cases, further investigation is needed to determine whether the issue lies in the shared encoder or the MBHB decoder head.

Regarding the estimation of astrophysical source parameters and their posterior distributions, our current approach is centered on source separation rather than direct Bayesian inference. The encoder-decoder framework extracts individual signals from a noisy mixture, producing separated outputs for each source. While this does not inherently yield posterior distributions, the extracted signals can serve as inputs to subsequent inference models. Future work will explore incorporating Bayesian techniques, such as neural density estimators (e.g., normalizing flows), to estimate posterior distributions of source parameters based on the separated signals. This will provide a more comprehensive understanding of uncertainties while leveraging the strengths of our blind source separation framework.

V. CONCLUSION

In this work, we presented a deep learning-based framework for blind source separation in high-dimensional LISA data, addressing overlapping

gravitational-wave signals and non-stationary noise artifacts. Inspired by `demucs`, a model originally designed for audio processing, our approach employs a shared encoder-decoder architecture to disentangle complex signal components directly in a single step, bypassing iterative subtraction techniques, which represents a conceptual shift in methodology. The model isolates individual components dynamically through latent space clustering while remaining scalable to high-density astrophysical populations.

The evaluation of our method on simulated LISA data demonstrated its ability to successfully handle challenging observational conditions, including high-redshift MBHB mergers embedded in realistic noise, overlapping glitches, and quiet periods devoid of mergers, thereby minimizing false positives.

Our current implementation is a proof-of-concept study, that restricts the number of overlapping GBs and excludes complicated EMRI waveforms. Nevertheless, the results demonstrate the potential of deep source separation for LISA data analysis. Notably, even with this simple framework – consisting of a few hundred lines of

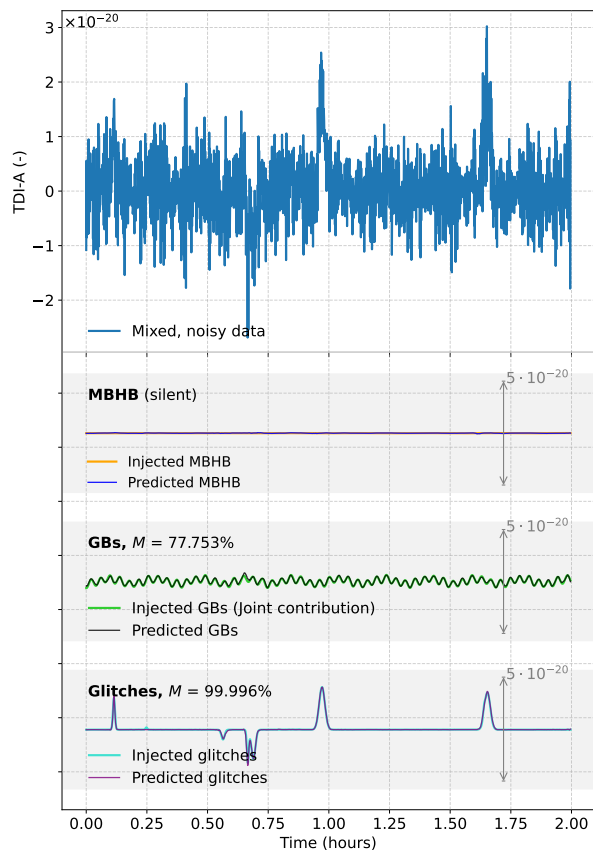


FIG. 8: Evaluation of the model in a time segment without a dominant MBHB to assess its ability to avoid false positives.

code and trained on a modest dataset – model inference operates efficiently on a standard laptop within seconds. Building on the presented results, we will explore the framework’s scalability to more complex, large-scale source populations. We are optimistic about its broader applicability.

As LISA’s launch approaches, scalable and efficient data analysis methods become increasingly important. Deep source separation offers a promising avenue for addressing the mission’s low-latency and global fit requirements, complementing traditional Bayesian inference and MCMC techniques. By refining and extending the method presented in this work, we aim to drive the development of next-generation gravitational wave detection strategies, setting a new standard for ML-based data analysis in our astrophysics community.

ACKNOWLEDGMENTS

This research was funded by the Gravitational Physics Professorship at ETH Zurich. The author thanks Michele Vallisneri for the insightful discussions and for his valuable contributions to editing the manuscript. Gratitude is also extended to the LISA Simulation Working Group and the LISA Simulation Expert Group for their engaging exchanges on all simulation-related activities. Copyright 2025. All rights reserved.

-
- [1] M. Colpi, K. Danzmann, M. Hewitson, K. Holley-Bockelmann, P. Jetzer, *et al.*, *LISA Definition Study Report* (2024), [arXiv:2402.07571](https://arxiv.org/abs/2402.07571) [astro-ph.CO].
 - [2] W. Martens and E. Joffre, Trajectory Design for the ESA LISA Mission, *The Journal of the Astronautical Sciences* **68**, 402 (2021).
 - [3] B. P. Abbott, R. Abbott, T. D. Abbott, M. R. Abernathy, F. Acernese, K. Ackley, C. Adams, T. Adams, P. Addesso, R. X. Adhikari, *et al.* (LIGO Scientific Collaboration and Virgo Collaboration), Observation of Gravitational Waves from a Binary Black Hole Merger, *Phys. Rev. Lett.* **116**, 061102 (2016).
 - [4] B. P. Abbott, R. Abbott, T. D. Abbott, M. R. Abernathy, F. Acernese, K. Ackley, C. Adams, T. Adams, P. Addesso, R. X. Adhikari, *et al.* (LIGO Scientific Collaboration and Virgo Collaboration), GW151226: Observation of Gravitational Waves from a 22-Solar-Mass Binary Black Hole Coalescence, *Phys. Rev. Lett.* **116**, 241103 (2016).
 - [5] B. P. Abbott, R. Abbott, T. D. Abbott, F. Acernese, K. Ackley, C. Adams, T. Adams, P. Addesso, R. X. Adhikari, V. B. Adya, *et al.* (LIGO Scientific and Virgo Collaboration), GW170104: Observation of a 50-Solar-Mass Binary Black Hole Coalescence at Redshift 0.2, *Phys. Rev. Lett.* **118**, 221101 (2017).
 - [6] B. P. Abbott, R. Abbott, T. D. Abbott, F. Acernese, K. Ackley, C. Adams, T. Adams, P. Addesso, R. X. Adhikari, and V. B. Adya, GW170608: Observation of a 19 Solar-mass Binary Black Hole Coalescence, *The Astrophysical Journal Letters* **851**, L35 (2017).
 - [7] B. P. Abbott, R. Abbott, T. D. Abbott, F. Acernese, K. Ackley, C. Adams, T. Adams, P. Addesso, R. X. Adhikari, and V. B. Adya (LIGO Scientific Collaboration and Virgo Collaboration), GW170814: A Three-Detector Observation of Gravitational Waves from a Binary Black Hole Coalescence, *Phys. Rev. Lett.* **119**, 141101 (2017).
 - [8] B. P. Abbott, R. Abbott, T. D. Abbott, F. Acernese, K. Ackley, C. Adams, T. Adams, P. Addesso, R. X. Adhikari, V. B. Adya, *et al.* (LIGO Scientific Collaboration and Virgo Collaboration), GW170817: Observation of Gravitational Waves from a Binary Neutron Star Inspiral, *Phys. Rev. Lett.* **119**, 161101 (2017).
 - [9] B. P. Abbott, R. Abbott, T. D. Abbott, S. Abraham, F. Acernese, K. Ackley, C. Adams, R. X. Adhikari, V. B. Adya, C. Affeldt, *et al.* (LIGO Scientific Collaboration and Virgo Collaboration), GWTC-1: A Gravitational-Wave Transient Catalog of Compact Binary Mergers Observed by LIGO and Virgo during the First and Second

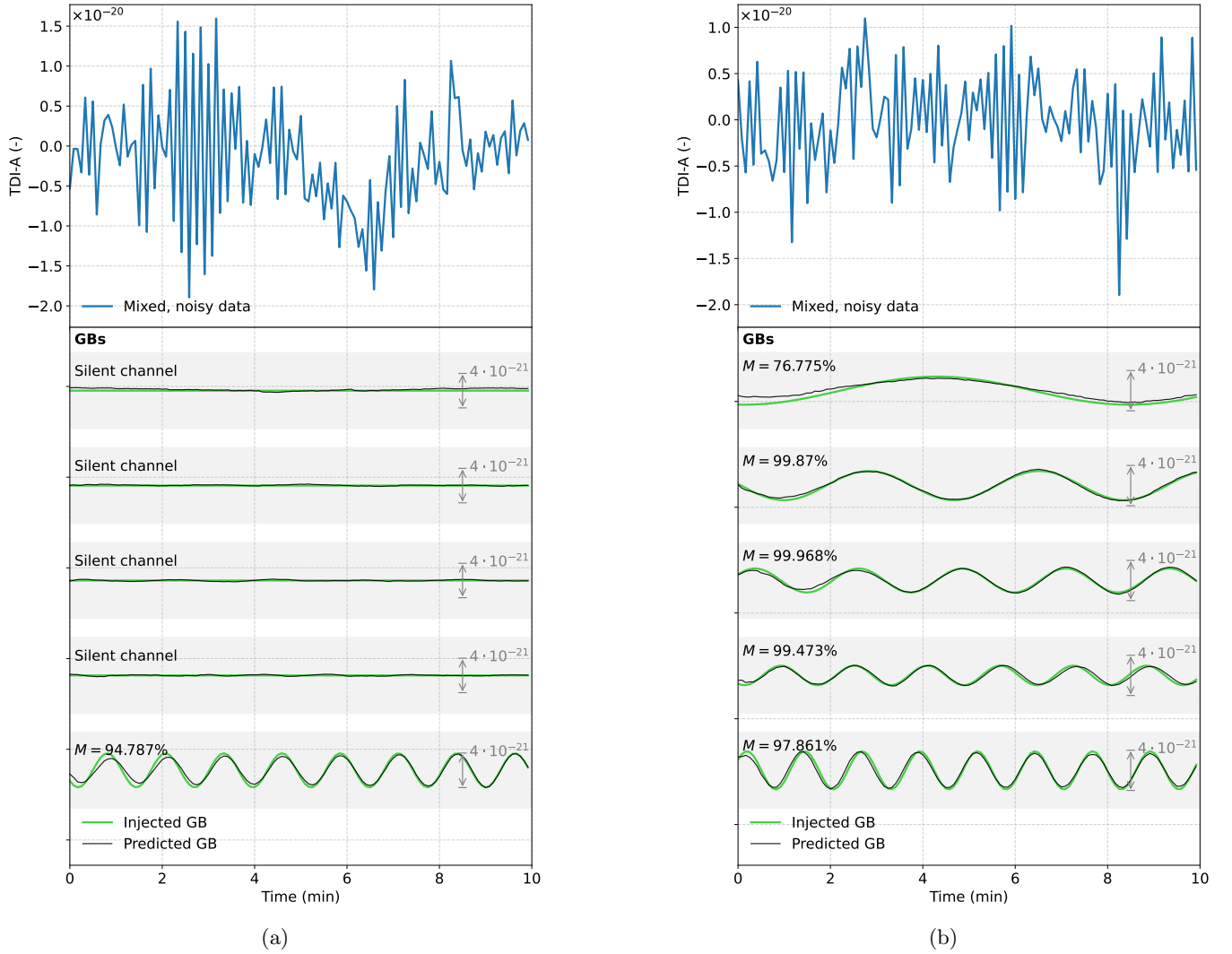


FIG. 9: Comparison of the injected and predicted GB waveforms in the presence of glitches. We do not highlight the injected glitches explicitly in the noisy input dataset. The multi-channel GB decoder accurately estimates the number of active GB sources, i.e., one in panel (a) and five in (b). Scaling to the thousands of overlapping GBs expected in LISA will require larger training datasets and deeper network architectures. The flexible framework developed in this work provides a solid foundation for such extensions.

- Observing Runs, *Phys. Rev. X* **9**, 031040 (2019).
- [10] B. P. Abbott, R. Abbott, T. D. Abbott, S. Abraham, F. Acernese, K. Ackley, C. Adams, R. X. Adhikari, V. B. Adya, C. Affeldt, *et al.*, GW190425: Observation of a Compact Binary Coalescence with Total Mass $\sim 3.4 M_{\odot}$, *The Astrophysical Journal Letters* **892**, L3 (2020).
- [11] R. Abbott, T. D. Abbott, S. Abraham, F. Acernese, K. Ackley, C. Adams, R. X. Adhikari, V. B. Adya, C. Affeldt, M. Agathos, *et al.* (LIGO Scientific Collaboration and Virgo Collaboration), GW190412: Observation of a binary-black-hole coalescence with asymmetric masses, *Phys. Rev. D* **102**, 043015 (2020).
- [12] R. Abbott, T. D. Abbott, S. Abraham, F. Acernese, K. Ackley, C. Adams, R. X. Adhikari, V. B. Adya, C. Affeldt, M. Agathos, *et al.*, GW190814: Gravitational Waves from the Coalescence of a 23 Solar Mass Black Hole with a 2.6 Solar Mass Compact Object, *The Astrophysical Journal Letters* **896**, L44 (2020).
- [13] R. Abbott, T. D. Abbott, S. Abraham, F. Acernese, K. Ackley, C. Adams, R. X. Adhikari, V. B. Adya, C. Affeldt, and M. Agathos (LIGO Scientific Collaboration and Virgo Collaboration), GW190521: A Binary Black Hole Merger with a Total Mass of $150 M_{\odot}$, *Phys. Rev. Lett.* **125**, 101102 (2020).
- [14] LISA Science Study Team, LISA Science Requirements document, Technical Report, European Space Agency (2018), technical Report ESA-L3-EST-SCI-RS-001.
- [15] P. Amaro-Seoane, S. Aoudia, S. Babak, P. Binétruy, E. Berti, A. Bohé, C. Caprini, M. Colpi, N. J. Cornish, K. Danzmann, *et al.*, Low-frequency gravitational-wave science with eLISA/NGO, *Classical and Quantum Gravity* **29**, 124016 (2012).
- [16] J. Crowder and N. J. Cornish, Solution to the galactic foreground problem for LISA, *Phys. Rev. D* **75**, 043008

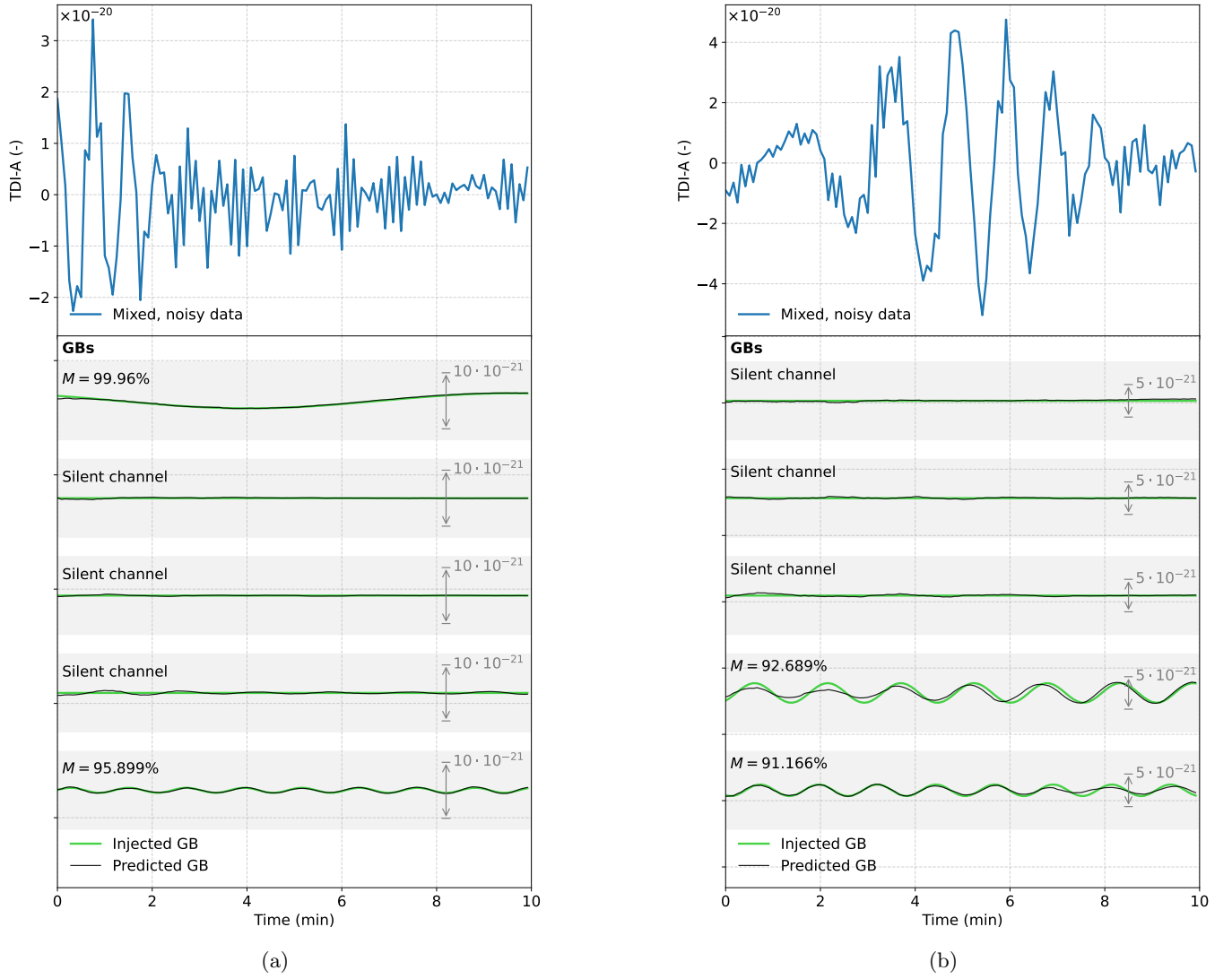


FIG. 10: Comparison of the injected and predicted GB waveforms in the presence of a merging MBHB. We do not highlight the injected MBHB explicitly.

- (2007).
- [17] A. W. Criswell, S. Rieck, and V. Mandic, Templated anisotropic analyses of the LISA Galactic foreground, *Phys. Rev. D* **111**, 023025 (2025), [arXiv:2410.23260 \[astro-ph.IM\]](https://arxiv.org/abs/2410.23260).
- [18] J.-B. Bayle, M. Lilley, A. Petiteau, and H. Halloin, Effect of filters on the time-delay interferometry residual laser noise for LISA, *Physical Review D* **99**, 084023 (2018).
- [19] S. Paczkowski, R. Giusteri, M. Hewitson, N. Karnesis, E. D. Fitzsimons, G. Wanner, and G. Heinzl, Postprocessing subtraction of tilt-to-length noise in LISA, *Phys. Rev. D* **106**, 042005 (2022).
- [20] N. Houba, *Tilt-to-Length Noise Estimation and Reduction Algorithms for Spaceborne Gravitational-Wave Observatories*, Fortschrittsberichte des Instituts für Flugmechanik und Flugregelung, Vol. 15 (Shaker Verlag, Düren, 2023) ISBN-9783844092813.
- [21] M. L. Katz, N. Karnesis, N. Korsakova, J. R. Gair, and N. Stergioulas, Efficient GPU-accelerated multisource global fit pipeline for LISA data analysis, *Phys. Rev. D* **111**, 024060 (2025).
- [22] T. B. Littenberg and N. J. Cornish, Prototype global analysis of LISA data with multiple source types, *Physical Review D* (2023).
- [23] S. H. Strub, L. Ferraioli, C. Schmelzbach, S. C. Stähler, and D. Giardini, Global analysis of LISA data with Galactic binaries and massive black hole binaries, *Phys. Rev. D* **110**, 024005 (2024).
- [24] P. J. Green, Reversible jump Markov chain Monte Carlo computation and Bayesian model determination, *Biometrika* **82**, 711 (1995), <https://academic.oup.com/biomet/article-pdf/82/4/711/699533/82-4-711.pdf>.
- [25] C. Ritter and M. A. Tanner, Facilitating the Gibbs Sampler: The Gibbs Stopper and the Griddy-Gibbs Sampler, *Journal of the American Statistical Association* **87**, 861–868 (1992).

- [26] P. Müller, *A Generic Approach to Posterior Integration and Gibbs Sampling*, Technical Report TR91-09 (Department of Statistics, Purdue University, 1991).
- [27] S. H. Strub, L. Ferraioli, C. Schmelzbach, S. C. Stähler, and D. Giardini, Bayesian parameter estimation of Galactic binaries in LISA data with Gaussian process regression, *Phys. Rev. D* **106**, 062003 (2022), [arXiv:2204.04467 \[astro-ph.IM\]](#).
- [28] D. Michelsanti, Z.-H. Tan, S.-X. Zhang, Y. Xu, M. Yu, D. Yu, and J. Jensen, An Overview of Deep-Learning-Based Audio-Visual Speech Enhancement and Separation, *IEEE/ACM Transactions on Audio, Speech, and Language Processing* **29**, 1368–1396 (2021).
- [29] E. Vincent, T. Virtanen, and S. Gannot, eds., *Audio Source Separation and Speech Enhancement* (John Wiley and Sons, Nashville, TN, 2018).
- [30] P. Ochieng, Deep neural network techniques for monaural speech enhancement and separation: state of the art analysis, *Artificial Intelligence Review* **56**, 3651–3703 (2023).
- [31] A. Tharwat, Independent component analysis: An introduction, *Applied Computing and Informatics* **17**, 222–249 (2020).
- [32] J. Thiemann and E. Vincent, An experimental comparison of source separation and beamforming techniques for microphone array signal enhancement, in *2013 IEEE International Workshop on Machine Learning for Signal Processing (MLSP)* (2013) pp. 1–5.
- [33] A. Wang, An Industrial Strength Audio Search Algorithm, in *International Society for Music Information Retrieval Conference* (2003).
- [34] H. Lee, M. Gwak, K. Lee, M. Kim, J. Konan, and O. Bhargava, *Speech Enhancement for Virtual Meetings on Cellular Networks* (2023), [arXiv:2302.00868 \[cs.SD\]](#).
- [35] S. Ansari, A. S. Alatrany, K. A. Alnajjar, T. Khater, S. Mahmoud, D. Al-Jumeily, and A. J. Hussain, A survey of artificial intelligence approaches in blind source separation, *Neurocomputing* **561**, 126895 (2023).
- [36] J.-T. Chien, *Source Separation and Machine Learning* (Academic Press, San Diego, CA, 2018).
- [37] A. Défossez, N. Usunier, L. Bottou, and F. Bach, Music Source Separation in the Waveform Domain (2019), working paper or preprint.
- [38] A. Mangiagli, C. Caprini, M. Volonteri, S. Marsat, S. Vergani, N. Tamanini, and L. Speri, Cosmology with massive black hole binary mergers in the LISA era., in *Proceedings of 41st International Conference on High Energy physics — PoS(ICHEP2022)*, ICHEP2022 (Sissa Medialab, 2022).
- [39] A. Mangiagli, C. Caprini, S. Marsat, L. Speri, R. R. Caldwell, and N. Tamanini, *Massive black hole binaries in LISA: constraining cosmological parameters at high redshifts* (2024), [arXiv:2312.04632 \[astro-ph.CO\]](#).
- [40] E. Leroy, J. Bobin, and H. Moutarde, Low-dimensional signal representations for massive black hole binary signals analysis from LISA data, *Astronomy; Astrophysics* **689**, A107 (2024).
- [41] T. Kupfer, V. Korol, T. B. Littenberg, S. Shah, E. Savalle, P. J. Groot, T. R. Marsh, M. Le Jeune, G. Nelemans, A. F. Pala, A. Petiteau, G. Ramsay, D. Steeghs, and S. Babak, *LISA Galactic Binaries with Astrometry from Gaia DR3* (2024).
- [42] N. Cornish and T. Robson, Galactic binary science with the new LISA design, *Journal of Physics: Conference Series* **840**, 012024 (2017).
- [43] K. Lackeos, T. B. Littenberg, N. J. Cornish, and J. I. Thorpe, The LISA Data Challenge Radler analysis and time-dependent ultra-compact binary catalogues, *Astronomy; Astrophysics* **678**, A123 (2023).
- [44] T. B. Littenberg and A. K. Lali, *Have any LISA verification binaries been found?* (2024), [arXiv:2404.03046 \[astro-ph.HE\]](#).
- [45] J. R. Gair, C. Tang, and M. Volonteri, Lisa extreme-mass-ratio inspiral events as probes of the black hole mass function, *Phys. Rev. D* **81**, 104014 (2010).
- [46] I. Qunbar and N. C. Stone, Enhanced Extreme Mass Ratio Inspirals Rates and Intermediate Mass Black Holes, *Phys. Rev. Lett.* **133**, 141401 (2024).
- [47] C. P. L. Berry, S. A. Hughes, C. F. Sopuerta, A. J. K. Chua, A. Heffernan, K. Holley-Bockelmann, D. P. Mihaylov, M. C. Miller, and A. Sesana, *The unique potential of extreme mass-ratio inspirals for gravitational-wave astronomy* (2019), [arXiv:1903.03686 \[astro-ph.HE\]](#).
- [48] A. Rüdiger, G. Heinzel, and M. Tröbs, LISA, the Laser Interferometer Space Antenna, Requires the Ultimate in Lasers, Clocks, and Drag-Free Control, in *Lasers, Clocks and Drag-Free Control* (Springer Berlin Heidelberg, 2008) p. 427–455.
- [49] G. Wanner, S. Shah, M. Staab, H. Wegener, and S. Paczkowski, In-depth modeling of tilt-to-length coupling in LISA’s interferometers and TDI Michelson observables, *Phys. Rev. D* **110**, 022003 (2024).
- [50] P. L. Bender, A. Brillet, I. Ciufolini, A. M. Cruise, C. Cutler, K. Danzmann, *et al.*, LISA. Laser Interferometer Space Antenna for the detection and observation of gravitational waves. An international project in the field of Fundamental Physics in Space, Max-Planck-Institut für Quantenoptik, München, Germany (1998), Pre-Phase A Report.
- [51] Q. Baghi, N. Korsakova, J. Slutsky, E. Castelli, N. Karnesis, and J.-B. Bayle, Detection and characterization of instrumental transients in LISA Pathfinder and their projection to LISA, *Phys. Rev. D* **105**, 042002 (2022).
- [52] E. Castelli, Q. Baghi, J. G. Baker, J. Slutsky, J. Bobin, N. Karnesis, A. Petiteau, O. Sauter, P. Wass, and W. J. Weber, *Extraction of gravitational wave signals from LISA data in the presence of artifacts* (2025), [arXiv:2411.13402 \[gr-qc\]](#).
- [53] N. Houba, L. Ferraioli, and D. Giardini, Detection and mitigation of glitches in LISA data: A machine learning approach, *Physical Review D* **109**, 10.1103/physrevd.109.083027 (2024).
- [54] M. Tinto, F. B. Estabrook, and J. W. Armstrong, Time-delay interferometry for LISA, *Physical Review D* **65**, 10.1103/physrevd.65.082003 (2002).
- [55] M. Tinto and S. V. Dhurandhar, Time-Delay Interferometry, *Living Reviews in Relativity* **8**, 10.12942/lrr-2005-4 (2005).
- [56] M. Vallisneri, J.-B. Bayle, S. Babak, and A. Petiteau, Time-delay interferometry without delays, *Phys. Rev. D* **103**, 082001 (2021).
- [57] K. Li, X. Hu, and Y. Luo, *On the Use of Deep Mask Estimation Module for Neural Source Separation Systems* (2022), [arXiv:2206.07347 \[cs.SD\]](#).
- [58] A. J. R. Simpson, Probabilistic Binary-Mask Cocktail-Party Source Separation in a Convolutional Deep Neural Network, *ArXiv abs/1503.06962* (2015).

- [59] M. Niu and Y. Zhang, Binaural Blind Source Separation Based on Deep Clustering, in *Advances in Natural Computation, Fuzzy Systems and Knowledge Discovery*, edited by H. Meng, T. Lei, M. Li, K. Li, N. Xiong, and L. Wang (Springer International Publishing, Cham, 2021) pp. 1077–1086.
- [60] M. Li, C. Cao, C. Li, and S. Yang, Deep Embedding Clustering Based on Residual Autoencoder, *Neural Processing Letters* **56**, [10.1007/s11063-024-11586-0](https://doi.org/10.1007/s11063-024-11586-0) (2024).
- [61] J. Xie, R. Girshick, and A. Farhadi, Unsupervised deep embedding for clustering analysis, in *Proceedings of the 33rd International Conference on International Conference on Machine Learning - Volume 48*, ICML'16 (JMLR.org, 2016) p. 478–487.
- [62] M. Moradi Fard, T. Thonet, and E. Gaussier, Deep k-Means: Jointly clustering with k-Means and learning representations, *Pattern Recognition Letters* **138**, 185 (2020).
- [63] Y. Luo, Z. Chen, J. R. Hershey, J. L. Roux, and N. Mesgarani, Deep clustering and conventional networks for music separation: Stronger together, *2017 IEEE International Conference on Acoustics, Speech and Signal Processing (ICASSP)*, 61 (2016).
- [64] T. Chang, B. P. Rasmussen, B. G. Dickson, and L. J. Zachmann, Chimera: A Multi-Task Recurrent Convolutional Neural Network for Forest Classification and Structural Estimation, *Remote Sensing* **11**, 768 (2019).
- [65] E. Manilow, P. Seetharaman, and B. Pardo, Simultaneous Separation and Transcription of Mixtures with Multiple Polyphonic and Percussive Instruments, in *ICASSP 2020 - 2020 IEEE International Conference on Acoustics, Speech and Signal Processing (ICASSP)* (2020) pp. 771–775.
- [66] T. Nakamura, S. Kozuka, and H. Saruwatari, Time-Domain Audio Source Separation With Neural Networks Based on Multiresolution Analysis, *IEEE/ACM Transactions on Audio, Speech, and Language Processing* **29**, 1687 (2021).
- [67] T. Nakamura and H. Saruwatari, Time-domain audio source separation based on wave-u-net combined with discrete wavelet transform, in *ICASSP 2020 - 2020 IEEE International Conference on Acoustics, Speech and Signal Processing (ICASSP)* (2020) pp. 386–390.
- [68] Y. Luo and N. Mesgarani, Conv-tasnet: Surpassing ideal time–frequency magnitude masking for speech separation, *IEEE/ACM Trans. Audio, Speech and Lang. Proc.* **27**, 1256–1266 (2019).
- [69] O. Ronneberger, P. Fischer, and T. Brox, U-net: Convolutional networks for biomedical image segmentation, in *Medical Image Computing and Computer-Assisted Intervention – MICCAI 2015*, edited by N. Navab, J. Hornegger, W. M. Wells, and A. F. Frangi (Springer International Publishing, Cham, 2015) pp. 234–241.
- [70] N. Tishby, F. C. Pereira, and W. Bialek, *The information bottleneck method* (2000), [arXiv:physics/0004057 \[physics.data-an\]](https://arxiv.org/abs/physics/0004057).
- [71] O. Ronneberger, P. Fischer, and T. Brox, U-net: Convolutional networks for biomedical image segmentation, in *Medical Image Computing and Computer-Assisted Intervention – MICCAI 2015*, edited by N. Navab, J. Hornegger, W. M. Wells, and A. F. Frangi (Springer International Publishing, Cham, 2015) pp. 234–241.
- [72] T. A. Prince, M. Tinto, S. L. Larson, and J. W. Armstrong, LISA optimal sensitivity, *Physical Review D* **66**, [10.1103/physrevd.66.122002](https://doi.org/10.1103/physrevd.66.122002) (2002).
- [73] T. T. Cai and R. Ma, Theoretical Foundations of t-SNE for Visualizing High-Dimensional Clustered Data, *Journal of Machine Learning Research* **23**, 1 (2022).
- [74] M. L. Katz, S. Marsat, A. J. K. Chua, S. Babak, and S. L. Larson, GPU-accelerated massive black hole binary parameter estimation with LISA, *Phys. Rev. D* **102**, 023033 (2020), [arXiv:2005.01827 \[gr-qc\]](https://arxiv.org/abs/2005.01827).
- [75] M. L. Katz, A fully-automated end-to-end pipeline for massive black hole binary signal extraction from LISA data (2021), [arXiv:2111.01064 \[gr-qc\]](https://arxiv.org/abs/2111.01064).
- [76] M. L. Katz, [mikekatz04/BBHx: First official public release](https://github.com/mikekatz04/BBHx) (2021).
- [77] N. J. Cornish and T. B. Littenberg, Tests of Bayesian model selection techniques for gravitational wave astronomy, *Phys. Rev. D* **76**, 083006 (2007).
- [78] K. Pearson, On lines and planes of closest fit to systems of points in space, *The London, Edinburgh, and Dublin Philosophical Magazine and Journal of Science* **2**, 559–572 (1901).
- [79] L. McInnes, J. Healy, N. Saul, and L. Großberger, UMAP: Uniform Manifold Approximation and Projection, *Journal of Open Source Software* **3**, 861 (2018).